Simulation of the current dynamics in superconductors: Application to magnetometry measurements

M. Zehetmayer*
Vienna University of Technology, Atominstitut, 1020 Vienna, Austria
(Received 12 May 2009; revised manuscript received 27 August 2009; published 25 September 2009)

A simple model for simulating the current dynamics and the magnetic properties of superconductors is presented. Short simulation times are achieved by solving the differential form of Maxwell's equations inside the sample, whereas integration is only required at the surface to meet the exact boundary conditions. The procedure reveals the time and position dependence of the current density and the magnetic induction (B) making it very convenient to apply field dependent material parameters for the simulation of magnetization loops, relaxation measurements, etc. Two examples, which are important for standard magnetometry experiments, are discussed. First, we prove that evaluating the critical current density (J_c) from experiment by applying Bean's model reveals almost the exact $J_c(B)$ behavior if the evaluation is corrected by a simple numerical expression. Second, we show that the superconducting volume fraction of a sample can be directly determined from magnetization loops by carefully comparing experiment and simulation in the field range, where the current loops are differently oriented within the sample.

DOI: 10.1103/PhysRevB.80.104512 PACS number(s): 74.25.Ha, 74.25.Sv, 02.60.Cb

I. INTRODUCTION

Simulating the magnetic behavior of type-II superconductors requires solving Maxwell's equations under specific material equations. Many different models have been proposed for solving this task including energy minimization, variational, or more direct approaches (e.g., Refs. 1–9). When addressing not only the static but also the dynamic behavior, it is often convenient to calculate the time evolution of field relevant quantities (e.g., of the magnetic vector potential or of the induction) directly.

Still, different approaches can be chosen. The most direct way is to solve Maxwell's equations by integration (i.e., with the help of the appropriate Green's function) which yields, e.g., the current density or the vector potential.[3] This method naturally leads to results fulfilling the electromagnetic boundary conditions at the sample surface. However, integrating over the whole sample volume requires a lot of calculation time and is usually too slow for three-dimensional (3D) problems. For a grid of N^3 elements, into which the sample is divided for the numerics, at least N^6 operations have to be performed per time step.

The opposite approach deals with the differential form of Maxwell's equations, where fields and currents are locally related by difference equations.[9] This makes the calculations very fast inside the sample since only about N^3 operations per time step are required. Care has to be taken, however, with the boundary conditions at the surface, which requires solving the equations also outside the sample up to distances, where the influence of the sample can be neglected.

As a compromise, we present a model, where the differential equations are applied to the sample interior, whereas the values at the sample boundaries are obtained by integrating over the sample volume yielding the correct boundary conditions. This requires N^3+6N^4 operations. It was already demonstrated[10] that the model worked sufficiently rapidly for 3D calculations on a standard personal computer (PC).

In this paper, we provide details of the method and discuss examples relevant for everyday magnetometry measurements. In Sec. II the simulation procedure and some technical aspects of the implementation are described. We start with a general model but concentrate in the following on rectangular samples, for which several tests were carried out. Section III is devoted to applications of the method to magnetometry [e.g., superconducting quantum interference device (SQUID) or vibrating-sample magnetometer (VSM)] measurements. We will verify the well known experimental evaluation of the critical current density from magnetization loops by applying Bean's model and introduce a simple way of determining the superconducting volume fraction of a sample.

II. SIMULATION MODEL

Our aim is to solve Maxwell's equations relevant for the magnetic properties of a superconductor. We assume superconductors without (nonsuperconducting) magnetic properties and initially ignore the reversible magnetization of the superconducting state. Thus, Maxwell's equations (in SI units) for vacuum may be applied,

$$\vec{\nabla} \cdot \vec{B} = 0, \tag{1}$$

$$\vec{\nabla} \times \vec{B} = \mu_0 \vec{J}, \tag{2}$$

$$\partial_t \vec{B} = -\vec{\nabla} \times \vec{E}. \tag{3}$$

The displacement current [Eq. (2)] is not considered. $\vec{B}$ denotes the magnetic induction, $\mu_0 = 4\pi \times 10^{-7}$ T m A^{-1} denotes the vacuum permeability, $\vec{J}$ denotes the current density, and $\vec{E}$ denotes the electric field. Generally, the vector quantities depend on time (t) and position ($\vec{r}$). The electric field is usually explicitly provided, e.g., as a function of current density, induction, and material specific parameters such as the critical current density to specify the superconducting properties of the material. It is directed parallel to $\vec{B} \times \vec{v}$, where $\vec{v}$

denotes the velocity of the vortices caused by the Lorentz force $\vec{J}\times\vec{B}$. In the following, we will address rather simple configurations, relevant for most magnetometry experiments, where the currents flow perpendicular to $\vec{B}$ and thus $\vec{E}$ and $\vec{J}$ are parallel. The more complicated situation, where $\vec{J}$ has also a (usually small) component parallel to $\vec{B}$, which can occur in the case of arbitrary field directions or irregular sample geometries, etc., is not considered. Recently, this problem was solved for simple configurations in the (static) Bean limit,[11,12] but it is currently not establish how to obtain more general results. For the simpler examples, discussed here, different kinds of material equations are available in the literature, which describe different materials and experimental situations (e.g., Refs. 13–15). Most prominent is the power law

$$E = E_c\left(\frac{J}{J_c}\right)^n, \tag{4}$$

which reproduces the flux creep behavior of type-II superconductors quite well. Here, E_c is the electric field criterion, J_c is the critical current density, and n is the so-called n value, which is a two-digit number in most cases. Very large n values (e.g., $n=\infty$) reproduce the Bean model[16] ($E=0$ for $J<J_c$ and $E=\infty$ for $J>J_c$). Both J_c and n may depend on $\vec{B}$ and other parameters.

A. Procedure

(i) Our starting point is a convenient initial state of the magnetic induction $\vec{B}(\vec{r},t)$ and the corresponding current density $\vec{J}(\vec{r},t)$ (satisfying $\vec{\nabla}\times\vec{B}=\mu_0\vec{J}$). Usually, we start with $\vec{B}=0$ and $\vec{J}=0$ in the whole sample or with the results of a previous simulation.

(ii) Next, we calculate the electric field—$\vec{E}(\vec{r},t)$—by applying the material equation [e.g., Eq. (4)] and

(iii) its curl, which corresponds to the time derivative of the induction [$\partial_t\vec{B}$, cf. Eq. (3)] and thus leads to

(iv) the induction of the next time step,

$$\vec{B}(\vec{r},t+\Delta t) = \vec{B}(\vec{r},t) + \partial_t\vec{B}(\vec{r},t)\Delta t, \tag{5}$$

where Δt denotes a small time increment. Equations (3) and (5) are only applied to the interior of the sample, whereas

(v) $\vec{B}(\vec{r},t)$ at the sample surface is obtained by integrating over the sample volume to fulfill the boundary conditions,

$$\vec{B}(\vec{r},t+\Delta t) = \mu_0[\vec{H}_a(\vec{r},t+\Delta t) + \vec{H}_s(\vec{r},t)], \tag{6}$$

with

$$\vec{H}_s(\vec{r},t) = \frac{1}{4\pi}\int d^3r'\frac{\vec{J}(\vec{r}',t)\times(\vec{r}-\vec{r}')}{|\vec{r}-\vec{r}'|^3}. \tag{7}$$

$\vec{H}_a$ is the applied field. Equation (6) is the only place where this quantity appears (i.e., $\vec{H}_a$ influences our calculations only via the surface).

(vi) Knowing $\vec{B}$ in the whole sample allows evaluating $\vec{J}(\vec{r},t+\Delta t)$ from Eq. (2). Note that $\vec{B}(\vec{r},t+\Delta t)$ [Eq. (6)] is calculated from $\vec{H}_s(\vec{r},t)$, which actually refers to the current distribution of the previous time step. This calculation could be repeated with the new currents $\vec{J}(\vec{r},t+\Delta t)$, but this was found to be unnecessary due to the small value of Δt.

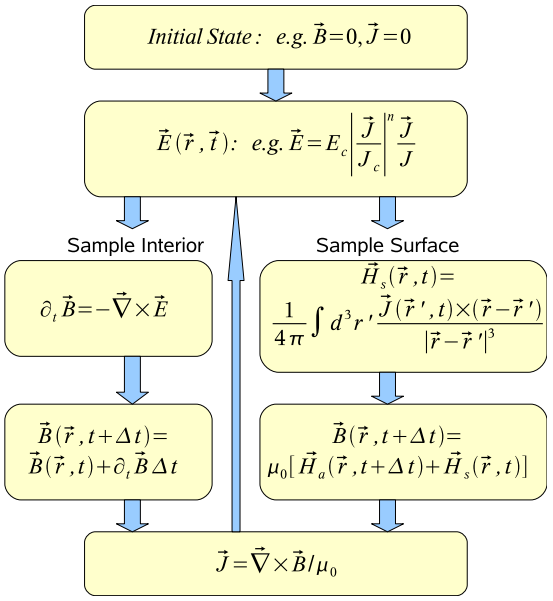

FIG. 1. (Color online) Flow diagram of the simulation sequence when only the *irreversible* magnetization is taken into account (see the text for details).

(vii) We end up with a new set of $\vec{B}$ and $\vec{J}$ close our simulation loop and proceed with calculating the next $\vec{E}$ [step (ii)].

Figure 1 outlines the major parts of the sequence. After the last step (vii) specific quantities may be evaluated (which is usually not done after each simulation loop but after predefined field or time intervals), e.g., the magnetic moment,

$$\vec{m} = \frac{1}{2}\int d^3r\vec{r}\times\vec{J}. \tag{8}$$

Thanks to the use of the difference equations, the simulations can be carried out quite rapidly. Time-consuming integration over the whole sample volume is only necessary for the induction at the sample surface to provide the correct boundary values.

We wish to point out another very attractive feature of this method, namely, the fact that the induction $\vec{B}$ is directly assessed in the simulations. This makes it very convenient to apply any field dependent property—in particular a field dependent critical current density $J_c(\vec{B})$—without the need of any additional calculations of $\vec{B}$ (as would be necessary for many other approaches).

Different specifications of $\vec{E}$ and $\vec{H}_a$ allow dealing with different materials and experiments. For instance, the simple power law of Eq. (4) leads to the typical flux creep behavior of superconductors. A transport current can be considered by adding external electric fields.

So far, only the irreversible properties have been addressed in the simulation procedure. A simple way of taking

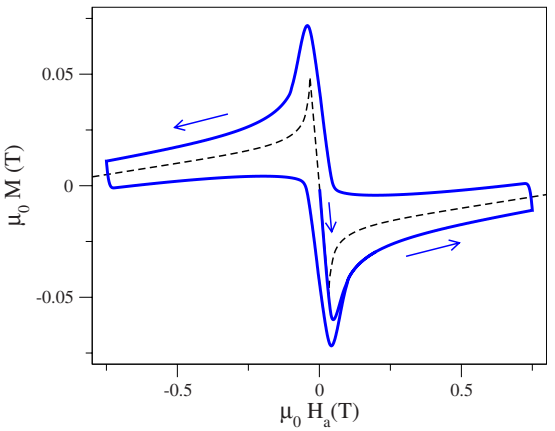

FIG. 2. (Color online) Simulation of the magnetization (solid line, $M=m/\mathrm{vol}$) of a superconductor ($a\times b\times c=1\times 1\times 1$ mm^3), where both the reversible and the irreversible contributions are significant. $J_c(B)$ is taken from Eq. (24) with $J_{c0}=2\times 10^8$ A m^{-2}, $B_0=0.02$ T, and $\alpha=0.5$. The dashed line illustrates the pure reversible fraction—$M_r(H_a)$ (obtained from the approximate equations in Ref. 17), where $B_{c2}=1$ T and $\kappa=4.8$—thus $B_{c1}\simeq 0.05$ T.

also the reversible magnetization of a superconductor into account is presented in Ref. 3, which can be easily adapted in our method by adding two further steps to the above procedure.

(viii) After finishing the last step (vii) of the original procedure, we know $\vec{B}$ and $\vec{J}$ in the entire sample. $\vec{B}$ is the overall local magnetic induction and thus includes also the contribution from the reversible magnetization $\vec{M}_r$, i.e.,

$$\vec{B}=\mu_0(\vec{H}+\vec{M}_r). \tag{9}$$

The reversible behavior may be assessed from Ginzburg Landau theory or from simpler approximations (like those in Ref. 17), which provide $\vec{M}_r$ as a function of $\vec{B}$ (or $\vec{H}$) and two parameters such as B_{c2}—the upper critical field—and κ—the Ginzburg Landau parameter. Note that $\vec{M}_r$ vanishes at the sample surface.

(ix) Equation (2) is still valid and the resulting $\vec{J}$ needed for calculating the boundary values [Eq. (7)]. Note that $\vec{J}$ includes also the reversible part of the currents and thus may be particularly large at the sample surface. However, $\vec{J}$ does not enter the Lorentz force density (f_L) that drives the flux lines, but[4] $f_L=\vec{J}_H\times\vec{B}$, with

$$\vec{\nabla}\times\vec{H}=\vec{J}_H, \tag{10}$$

where $\vec{H}$ is obtained from Eq. (9). Accordingly, $\vec{J}_H$ (but not $\vec{J}$) generates the electric field and we have to replace $\vec{J}$ by $\vec{J}_H$ in the expression for $\vec{E}$ (i.e., in the material equation). If the reversible magnetization is ignored (as, e.g., in the flow chart of Fig. 1), $\vec{M}_r=0$ and thus $\vec{J}=\vec{J}_H$.

Step (ix) finishes the procedure in case the reversible magnetization is not ignored, and we can proceed with step (ii). Figure 2 presents an example of a magnetization loop,

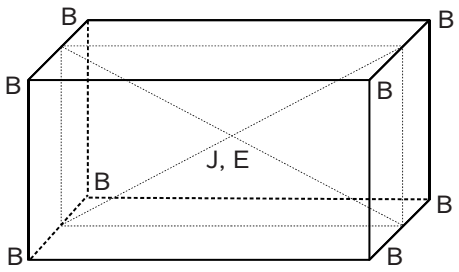

FIG. 3. Schematic view of a single element (in which $\vec{J}$ is constant) and the positions, where $\vec{B}$, $\vec{E}$, and $\vec{J}$ are calculated. The dotted square indicates the two-dimensional case (see the text for details).

where both the reversible and irreversible contributions are significant. For describing flux line motion we employ

$$\vec{E}=A_cB\frac{(J_H/J_c)^n}{1+(J_H/J_c)^n}\vec{J}_H, \tag{11}$$

as suggested in Ref. 3, which correctly leads to flux flow ($E\propto BJ_H$) at $J_H\gg J_c$ and flux creep at $J_H\ll J_c$. Here, A_c is an appropriate constant, equivalent to E_c of Eq. (4), but given in units of V m T^{-1} A^{-1}.

In the following, we mainly concentrate on samples with high critical current density, where the reversible properties may be ignored and therefore only steps (i)–(vii) will be executed.

B. Technical aspects

In this section, we address some specific points of our implementation. In most cases, we deal with rectangular samples and, therefore, subdivide the sample into small rectangular elements within which the current density is kept constant. For simplicity, we work with an equidistant grid but note that a better efficiency is expected from a grid with smaller elements near the surface since most quantities typically exhibit larger variations there. Each grid element consists of eight vertices and a central point (Fig. 3). The sequence (Fig. 1) dictates the position, on which each quantity is evaluated, in a natural way (Fig. 3). The induction $\vec{B}$ is defined at the vertices, which also include the sample surface. Accordingly, its derivative (or actually its curl) is calculated at the midpoint position using $\vec{B}$ values of the next eight adjacent vertices. The electric field is in most cases a direct function of the currents [e.g., Eq. (4)] and is therefore also calculated at the center of the elements. In the next step, we need the curl of $\vec{E}$, which naturally leads us back to the vertices and the results ($\partial_t\vec{B}$) immediately allow modifying $\vec{B}$ at those positions. Note that calculating the curl of $\vec{E}$ at the sample surface is not required.

At the sample surface, the induction is obtained by integration, which is approximated by a summation over the discrete elements k within which J is constant. The three components (x, y, and z) of Eq. (7) may be written as

$$H_{s,x}(\vec{r}_s) = \sum_k [J_y^{(k)} A_z^{(k)}(\vec{r}_s) - J_z^{(k)} A_y^{(k)}(\vec{r}_s)], \quad (12)$$

$$H_{s,y}(\vec{r}_s) = \sum_k [J_z^{(k)} A_x^{(k)}(\vec{r}_s) - J_x^{(k)} A_z^{(k)}(\vec{r}_s)], \quad (13)$$

$$H_{s,z}(\vec{r}_s) = \sum_k [J_x^{(k)} A_y^{(k)}(\vec{r}_s) - J_y^{(k)} A_x^{(k)}(\vec{r}_s)]. \quad (14)$$

The sums run over all elements of the grid, $J_i^{(k)}$ denotes the i component ($i=x$, y, or z) of the current density of the kth element, and $A_i^{(k)}(\vec{r}_s)$ denotes the i component of the function

$$\vec{A}^{(k)}(\vec{r}_s) = \frac{1}{4\pi} \int_{(k)} d^3r' \frac{\vec{r}_s - \vec{r}'}{|\vec{r}_s - \vec{r}'|^3}, \quad (15)$$

where $\vec{r}_s$ denotes a vertex position at the sample surface and the integral is performed over the volume of the kth element. We point out that it is essential to calculate these integrals numerically very accurately. Note, however, that $\vec{A}^{(k)}(\vec{r}_s)$ depends only on the position vectors; hence the integrals need to be calculated just once during the initial stage and can be stored for later use in Eqs. (12)–(14).

Finally, we address the problem of choosing an adequate time increment Δt, which should be as large as possible to make the simulation time short but small enough to have no influence on the results. In our implementation, it turns out that choosing Δt too large makes the calculations unstable with $|\vec{J}|$ increasing rapidly toward infinity. This situation can be easily monitored and mitigated by resuming the simulation from a previously saved configuration with a smaller Δt. It turns out that even smaller values of Δt do not modify the results.

C. Magnetization loops of rectangular samples

The model was successfully applied to fully 3D calculations in conveniently short simulation times, as reported in Ref. 10. In the following, we focus on magnetization loops of rectangular samples in the presence of a homogeneous external field, which occurs in most magnetometry experiments (e.g., SQUID or VSM). The external field is applied in z direction, perpendicular to the top and bottom surfaces of our sample, and we assume isotropic material parameters (e.g., J_c) within the xy plane. In this case, the model may be simplified assuming the currents to flow exactly parallel to the nearest sample surfaces. The benefits of the procedure are still available in the two-dimensional (2D) calculations, making it possible to simulate realistic magnetization loops very rapidly (e.g., within about 1–10 min on a conventional standard PC). We point out that our assumption on the current flow is not rigorously valid (see Ref. 18), but the deviations are only significant in very thin samples, which are not addressed here.

For the actual implementation, we assume the sample center to coincide with the point of origin and the lateral surfaces to be parallel to the x or y axis. The fields and currents need to be calculated only at the cross section spanned by the z and y axes, on which a 2D grid is defined. Thus we apply almost the same procedure as illustrated in Fig. 3 but mapped on two-dimensional elements (i.e., the cross section of each 3D element—see Fig. 3). The calculation of the surface field [Eqs. (12)–(14)] is slightly modified to

$$H_{s,x}(\vec{r}_s) = 0, \quad (16)$$

$$H_{s,y}(\vec{r}_s) = \sum_m J^{(m)} C_y^{(m)}(\vec{r}_s), \quad (17)$$

$$H_{s,z}(\vec{r}_s) = \sum_m J^{(m)} C_z^{(m)}(\vec{r}_s), \quad (18)$$

with

$$\vec{C}^{(m)}(\vec{r}_s) = \frac{1}{4\pi} \int_{(m)} d^3r' \frac{\vec{\epsilon}_J \times (\vec{r}_s - \vec{r}')}{|\vec{r}_s - \vec{r}'|^3}. \quad (19)$$

$H_{s,x}(\vec{r}_s)$ vanishes due to the symmetry of the system. The sums run over all two-dimensional elements (m) of the sample cross section. The integration is performed over one element (m) and—for the third dimension—over the closed current loop exactly parallel to the nearest sample surfaces. $\vec{\epsilon}_J$ indicates the unit vector of the *a priori* known current flow direction. Thus $\vec{C}^{(m)}(\vec{r}_s)$ can also be accurately calculated during the initial stage and stored for later use.

D. Tests of the simulations

Several tests are available for verifying the output of the simulations. The first concerns $H^\star$, the lowest applied field of a virgin $m(H_a)$ curve, at which the currents have penetrated the entire sample. It corresponds to the z component of the field of that current distribution at the center of the sample, which is easily calculated for constant currents [Bean model, e.g., Eq. (7), but with $\vec{r}=(0,0,0)^T$].

The simulations reveal $H^\star$ by monitoring the current density at the sample center. The Bean model is approximated by applying constant currents and—to reduce relaxation—a large n value. As expected, the deviation of $H^\star$ from the direct calculation is reduced with increasing n value and almost vanishes (smaller than 1%) at $n>100$.

Second, we can test the creep behavior of the currents by studying the relaxation of the magnetic moment. This time, the power law [Eq. (4)] was applied with a field dependent critical current density and a constant n value ($n=20$). Imitating the common experimental procedure, we started with simulating (parts of) a magnetization loop, followed by recording the relaxation in the fully penetrated state, i.e., the time dependence of the magnetic moment—$m(t)$—at constant applied field [Fig. 4(a)]. According to theory the n value may be extracted via $|d \ln m / d \ln t| \simeq 1/n$ which matches very well ($\sim$1.5% deviation) the input value of n in the simulation [see inset of Fig. 4(a)].

A second way of studying relaxation is provided by the so-called dynamic relaxation, where magnetization loops are measured (or simulated) at different field sweep rates $\dot{H}_a = dH_a/dt$ [Fig. 4(b)]. The relaxation rate at constant applied

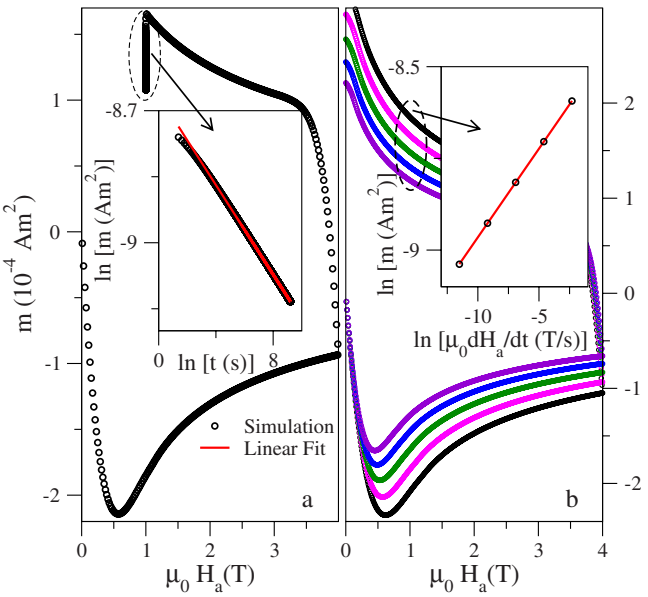

FIG. 4. (Color online) Verification of the creep behavior in the simulations. Panel (a) present a magnetization loop ($n=20$) followed by recording relaxation at 1 T for about 3 h. The inset shows the relaxation rate $d \ln m/d \ln t(\simeq -1/n)$ together with a linear fit revealing $n=19.7$. Panel (b) shows magnetization loops at different field sweep rates (10^{-5}, 10^{-4}, 10^{-3}, 10^{-2}, and 10^{-1} T/s) and the inset the dynamical relaxation rate $d \ln m/d \ln \mu_0 \dot{H}_a(\simeq 1/n)$ at 1 T, where the linear fit leads to $n=20.7$.

field is now given by $|d \ln m/d \ln \mu_0 \dot{H}_a| \simeq 1/n$ and is again found to be in good agreement ($\sim 3.5\%$ deviation) with our input value of n [see inset of Fig. 4(b)].

III. APPLICATION TO MAGNETOMETRY

A. Evaluation of the critical current density

1. Experiment

In the following we present two applications of the simulations to common problems of magnetometry experiments. The first refers to the evaluation of the critical current density from magnetization loops. Usually the Bean model is applied, which presumably leads to certain deviations from the correct J_c behavior. To analyze these deviations quantitatively we start from a given $J_c(B)$ behavior and simulate magnetization loops. Then we apply the same evaluation procedure as used for the experimental data to re-evaluate J_c, which is finally compared with our input J_c curve.

We start by explaining the experimental procedure used in most experiments for acquiring $J_c(H_a)$ from magnetometry measurements and introduce a simple extension that allows us to obtain $J_c(B)$. When determining the critical current density from SQUID or VSM measurements we usually do not know more than the magnetic moment as a function of applied field, $m(H_a)$, and the sample dimensions a, b, and c, where we assume c to be parallel to H_a. Thus, assumptions on J_c are inevitable, which are in most cases a constant absolute value of $\vec{J}$ equals J_c and a flow direction parallel to the nearest sample surfaces (Bean model). The relation between m and J_c is given by Eq. (8) leading to an analytic expression for rectangular samples in the fully penetrated state[19] that can be solved for J_c,

$$J_c = \frac{|m_i|}{\Omega} \frac{4}{b\left(1 - \frac{b}{3a}\right)} \quad \text{with } a \geq b, \tag{20}$$

where $\Omega = abc$ and m_i denotes the irreversible magnetic moment generated by the critical currents, which is given by half of the hysteresis width of the magnetization loop. Equation (20) leads to a first approximation of J_c as a function of the applied field—$J_c(H_a)$. To come closer to the actual material property, i.e., the critical current density as a function of the magnetic induction—$J_c(B)$—(which is independent of sample geometry), we additionally consider the field induced by the current distribution (cf. Ref. 20 for the case of cylindrical samples). Since the magnetic moment acquired by the magnetometry measurements always refers to the whole sample volume, the induction needs to be averaged in the same way to obtain $m(B)$, i.e.,

$$B = \mu_0 \langle |H_a + H_{s,z}| \rangle \tag{21}$$

with $\vec{H}_s$ from Eq. (7) and

$$\langle |H_a + H_{s,z}| \rangle = \frac{1}{w} \int d^3 r (\vec{r} \times \vec{\epsilon}_j)_z |H_a + H_{s,z}(\vec{r})|. \tag{22}$$

The integral runs over the whole sample volume. $(\vec{r} \times \vec{\epsilon}_j)_z$ represents a weighting factor, which corresponds to that of J_c in the calculation of m [cf. Eq. (8)] and reflects also the distance from the current element to the pick-up coils of the magnetometry devices. w is the integral of this factor over the sample volume. The weighting does not strongly affect the results but is still significant for the behavior of $J_c(B)$. Note further that we evaluate J_c as a function of the absolute value of the B component parallel to the applied field (B_z).

Finally, we address the evaluation of m_i. The experiments provide $m(H_a)$, which is usually the sum of m_i and of the reversible magnetic moment m_r. Additional magnetic signals from the sample or the sample holder can usually be treated in a similar way as m_r. m_i is extracted from (half of) the difference of m at increasing (H_+, B_+) and decreasing (H_-, B_-) fields at the same induction B. But note that the two branches of $m(H_a)$ refer to different values of B at the same H_a since the currents have opposite orientation in the two branches. Two situations are distinguished. First, when the irreversible part dominates, as is the case in most experiments, B is separately calculated for each branch of $m(H_a)$ by applying Eqs. (20) and (21) with $m_i \simeq m$. Then $m_i(B)$ is obtained from

$$m_i(B) = \frac{m(B_-) - m(B_+)}{2} \tag{23}$$

and the final $J_c(B)$ by evaluating Eq. (20) again. In the second case, where the reversible parts are significant or even dominate, the critical current density is usually low and therefore the corresponding field correction $(H_{s,z})$ is small.

Accordingly, we start with evaluating $m_i(H_a)=0.5[m(H_{a-})-m(H_{a+})]$, i.e., the irreversible magnetic moment from the hysteresis width at the same applied field, and then apply Eqs. (20) and (21) for getting $J_c(B)$.

2. Simulation

The above experimental evaluation is not expected to result in the "true" $J_c(B)$ curve. The main reason for discrepancies is the (necessary) assumption of a constant current density within the sample, which is not fulfilled in realistic materials, since B may vary considerably and $J_c(B)$ is usually not constant. Accordingly, we expect more pronounced deviations, when the samples are large and have high J_c, since both properties would enhance the (peak to peak) variation in B within the sample. At low fields this variation is comparable with $\mu_0 H^\star$, which may amount to several tesla in typical "SQUID or VSM" samples. At higher fields, we expect better agreement with the true J_c since J_c becomes smaller and flatter as a function of B in most cases.

To get some idea of the quantitative differences between the true J_c and J_c from the above evaluation, we simulated a typical magnetometry measurement assuming a sample size of $1\times1\times1$ mm^3 and a J_c behavior described by

$$J_c(B) = \frac{J_{c0}}{(1+B/B_0)^\alpha}. \tag{24}$$

Setting $B_0=0.2$ T and $\alpha=1/2$ roughly leads to a behavior observed in many (melt textured) $Y_1Ba_2Cu_3O_{7-x}$ (Y-123) samples at low temperatures. $J_{c0}=1\times10^{10}$ A m^{-2} leads to $\mu_0 H^\star \simeq 2.1$ T and a similarly large variation in B in the sample.

Furthermore, we applied the power law [Eq. (4)] with $E_c=5\times10^{-6}$ V m^{-1} and $n=20$ and a field sweep rate of $\mu_0\dot{H}_a=1\times10^{-2}$ T s^{-1}. This rather fast field sweep rate corresponds to the maximum we can set in our VSM measurements and was chosen to reduce relaxation effects, i.e., to get $J\simeq J_c$, where J is the real flowing current.

The inset of Fig. 5(a) presents the simulated magnetization curve of this sample up to fields of 9 T, including the virgin curve. Before applying the methods of Sec. III A 1, all parts of the curve, where the currents do not flow in the whole sample or do not have the same orientation, need to be removed. This is done automatically by the evaluation program and includes the appropriate parts of the virgin curve (i.e., for $H_a<H^\star$) and those parts directly after reversing the field, where the currents have opposite orientation.

The results are illustrated in Fig. 5(a). The open symbols show the original (input) $J_c(B)$, i.e., the true $J_c(B)$, according to Eq. (24). The dotted line presents $J_c^e(H_a)$, where the superscript "e" indicates that J_c has been evaluated from the magnetization curve [of the inset of Fig. 5(a)] with the (experimental) methods in Sec. III A 1, and the solid line is the final result $J_c^e(B)$ when considering also the field correction according to Eq. (21). $J_c^e(H_a)$ shows significant deviations from $J_c(B)$ at fields $H_a<H^\star$. $J_c^e(B)$, however, matches quite well despite the rather rough assumption of a constant current density in the sample (note that the peak to peak variation in B in the sample reaches 2.4 T at constant applied field in this specific simulation). Slower field sweep rates or field-step measurements would shift the curves to slightly smaller values due to relaxation. Note further that the evaluation method does not give access to J_c at or close to $B=0$ since the mean induction [cf. Eq. (22)] is always larger than zero.

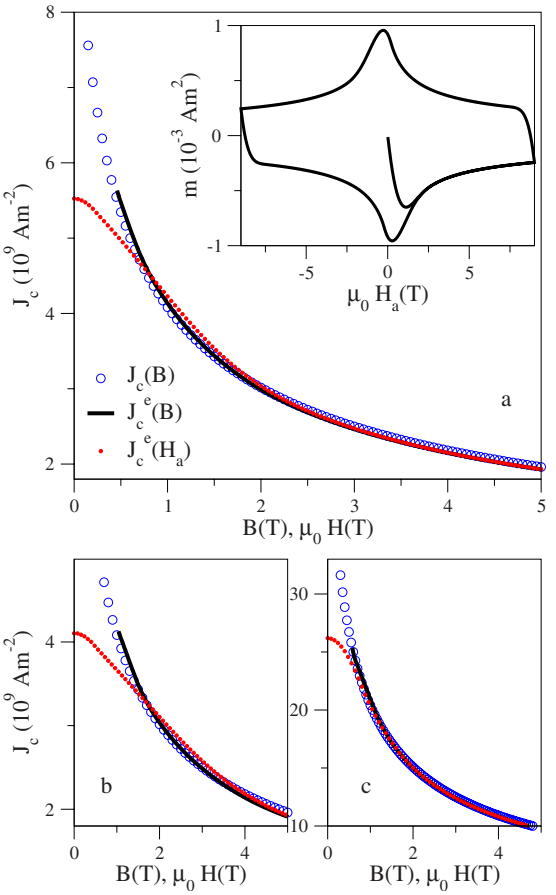

FIG. 5. (Color online) Results for different sample geometries: $a\times b\times c=1\times1\times1$ mm^3 in (a), $3\times3\times3$ mm^3 in (b), and $1\times0.5\times0.1$ mm^3 in (c). The open symbols show the input $J_c(B)$ used to simulate the magnetization loops [e.g., inset of (a)], the dotted curve $J_c(H_a)$, and the solid line $J_c(B)$ evaluated from the magnetization curves by using Bean's model (see text).

To get further insight, we repeated the procedure for different samples and $J_c(B)$ curves (e.g., with exponential behavior) and found similarly good agreement as above. For instance, Fig. 5(b) shows results on a sample with dimensions $3\times3\times3$ mm^3 and the same $J_c(B)$ as in the above example (only E_c is slightly adapted to account for the larger sample size). Although $\mu_0 H^\star$ of 4.4 T is quite large and $J_c^e(H_a)$ starts to deviate from $J_c(B)$ at a similarly high field, these deviations are again nicely corrected by $J_c^e(B)$.

Analyzing situations with much larger $\mu_0 H^\star$ does not make sense since the evaluation of J_c requires external fields larger than $\mu_0 H^\star$, but typical experimental devices do not provide fields much above 5–10 T. Increasing $J_c(B)$ instead of the sample size leads to similar effects.

As a final example, we show results on a sample with a size of $1\times0.5\times0.1$ mm^3, which is representative for a typical single crystal geometry. We took the same $J_c(B)$ behavior as in the above examples but with $J_{c0}=5\times10^{10}$ A m^{-2}, ac-

cordingly $\mu_0 H^\star \simeq 2.1$ T. Figure 5(c) presents the results, which again demonstrate the excellent agreement between the evaluated $J_c^e(B)$ and the input curve $J_c(B)$.

B. Superconducting volume fraction

The evaluation of the critical current density as described in the previous sections is only valid if the current flow is unimpeded over the whole sample. This is illustrated by Eq. (20), which shows that a sample with dimensions $a \times b \times c$ would induce a larger magnetic moment than the sum of two samples with dimensions $a \times b/2 \times c$, with the same J_c as the large sample. Thus, grain boundaries and other macroscopic inhomogeneities (e.g., normal conducting inclusions), which impede the current flow, would lead to an underestimation of J_c when applying the above method. A similar effect is caused by overestimating the superconducting sample volume, e.g., when the material properties are degraded at the surface. We further note that magnetization measurements are not only used for evaluating J_c but also for determining all kinds of superconducting parameters, such as the critical magnetic fields or the characteristic lengths, etc. (e.g., Ref. 21). Most of these quantities are derived from the magnetization, $M=m/\Omega$, i.e., it is again important to exactly know the volume (Ω). We point out that both surface degradation and grain boundaries were even found in samples believed to be single crystals. In the following we show that the reverse branch of a magnetization loop is very sensitive to such imperfections and that we can prove whether or not a sample is single grained and even detect if parts of the surface are degraded.

We started our analysis with experimental magnetization loops of a Y-123 sample at 30 K. The size of the rectangular sample was precisely measured with an optical microscope and found to be $a \simeq 1.44$ mm, $b \simeq 0.88$ mm, and $c \simeq 0.76$ mm. Using these data, $J_c(B)$ was calculated with the above method (Sec. III A 1), and the result was used for simulating the magnetization loops. As expected, there is agreement with experiment over most part of the field range. Small differences are only observed near $H_a=0$ since J_c close to $B=0$ needs to be extrapolated. We are, however, not interested in this region but look closer to that part of the reverse branch of the loop, where currents with opposite orientation flow in the sample (indicated by the two arrows in Fig. 6) and which had been disregarded for evaluating J_c. As shown in Fig. 6 there is perfect agreement between experiment (open circles) and simulation (solid line, $a \times b = 1.44 \times 0.88$ mm^2) even in this part of the loop, thus demonstrating that the size of the sample surface had been determined correctly and that the sample is pretty homogeneous for the macroscopic current flow. Comparing only the magnetization slope directly after the reversal point (up arrow in Fig. 6) (inset of Fig. 6) provides information on the sample size and surface but not on the interior since the newly penetrating currents (which have opposite orientation with respect to the existing currents) flow only at the sample surface. With decreasing applied field, the new currents penetrate into the sample and as soon as the current front reaches a region with a different J_c (e.g., at a grain boundary or a normal conducting inclusion) the macroscopic current path and therefore also the magnetic moment would start to deviate from the simulations (where perfect homogeneity is assumed). In addition, the field, where the new currents arrive at the center (down arrow in Fig. 6), would be different. To conclude, only comparing experiment and simulation over the whole penetration interval (i.e., form the up to the down arrow in Fig. 6) can clarify if samples are homogeneous (at least for the current flow) over the whole volume.

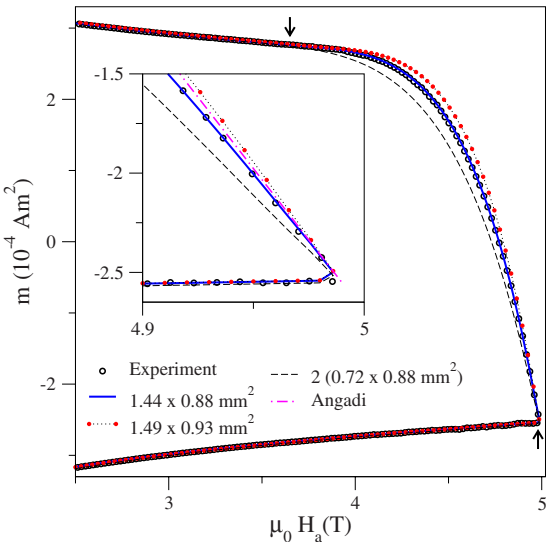

FIG. 6. (Color online) Comparison of the magnetic moment from experiment and simulations with different sample surface sizes. The arrows indicate the interval, within which currents with opposite orientation flow in the sample.

Let us assume that the measurement of the sample size had resulted in slightly larger values, namely, $a=1.49$ mm and $b=0.93$ mm, i.e., only 0.05 mm for both lengths, which increases the volume by about 9%. We repeated the whole procedure with these data (which leads to a slightly smaller J_c) and find again agreement on most parts of the $m(H_a)$ loops. However, inspecting the reverse branch more closely, we find significant disagreement between the two arrows (Fig. 6), i.e., where not all currents are equally oriented, which demonstrates different sample sizes. This indicates either an error in the measurement of the sample size or the fact that small regions of the lateral surfaces are nonsuperconducting. While a smaller J_c hardly affects the slope of $m(H_a)$ close to the reversal point, the larger sample size and the correspondingly larger current loop enhance the (absolute value of the) slope by about 10% as shown in the inset of Fig. 6 (note that $H^\star$ also increases).

Second, we studied the case of a sample divided into two independent grains (bicrystal) with sizes of $0.72 \times 0.88 \times 0.76$ mm^3 (i.e., $a/2 \times b \times c$). Since the relative contribution of the critical currents to the magnetic field is small at high applied field, any interaction between the two grains (i.e., magnetic fields from the other grain) was neglected. Having the same overall magnetic moment (which is simply the sum of m from the two grains) leads to a larger J_c than in the large (single grained) sample. As expected, the slope of $m(H_a)$ at the reversal point is significantly flatter in the

bicrystal (about 17%) than in the single grain sample (inset of Fig. 6) making it easy to distinguish between the different situations.

Finally, we compare our results on the slope of the reverse branch with the well known analytical expression given by Angadi *et al.*,[22] i.e., $dm/dH=-\pi^2R^3/\Theta$, with $\Theta=\ln(8R/c)-0.5$ and R as the radius of a cylinder which has the same surface area as the cuboid. Using this method results in a slope that deviates from simulation and experiment by only about 5% (inset of Fig. 6). However, applying the same method to the bicrystal leads to a slope that actually matches the exact result of the single grain sample even better. Thus, this approximation cannot be recommended to verify if samples are single grained or decomposed into a few grains.

IV. SUMMARY

Details of a simple method for two- or three-dimensional simulations of the current dynamics in a superconductor have been presented. Solving the differential form of Maxwell's equations in the sample interior makes the calculations very fast. The integral form is only used at the sample surfaces to meet the correct boundary conditions. The procedure results in the time and position dependence of the magnetic induction and the current density, which makes it very convenient to apply field dependent material parameters, such as $J_c(B)$. The method allows simulating different kinds of experiments, such as magnetization loops, static and dynamic relaxation measurements, etc., in which also the reversible superconducting properties may be considered.

To demonstrate the potential of the method, we presented two examples, which are important for standard magnetometry measurements. In the first, magnetization loops were simulated by applying a given $J_c(B)$ and then evaluated by the methods usually applied to experimental data, i.e., the Bean model. Comparison of the given $J_c(B)$ and the "Bean" $J_c(B)$ shows good agreement even for large samples and high J_c if the Bean result is corrected by a simple numerical expression.

Second, we showed that surface degradations, which reduce the superconducting volume fraction of a sample, or inhomogeneities such as grain boundaries, which influence the current flow, can be detected by carefully comparing the magnetization loops from experiment and simulation at regions, where currents with opposite orientation flow in the sample.

ACKNOWLEDGMENTS

I wish to thank Franz Sauerzopf and Harald W. Weber for helpful discussions. This work was supported by the Austrian Science Fund under Contract No. 21194.

*zehetm@ati.ac.at

[1] L. Prigozhin, J. Comput. Phys. **129**, 190 (1996).
[2] E. H. Brandt, Phys. Rev. B **54**, 4246 (1996).
[3] E. H. Brandt, Phys. Rev. B **59**, 3369 (1999).
[4] R. Labusch and T. B. Doyle, Physica C **290**, 143 (1997).
[5] A. Sanchez and C. Navau, Phys. Rev. B **64**, 214506 (2001).
[6] A. Badía and C. López, Phys. Rev. B **65**, 104514 (2002).
[7] A. M. Wolsky and A. M. Campbell, Supercond. Sci. Technol. **21**, 075021 (2008).
[8] A. M. Campbell, Supercond. Sci. Technol. **22**, 034005 (2009).
[9] Y. Lu, J. Wang, S. Wang, and J. Zheng, J. Supercond. Novel Magn. **21**, 467 (2008).
[10] M. Zehetmayer, M. Eisterer, and H. W. Weber, Supercond. Sci. Technol. **19**, S429 (2006).
[11] G. P. Mikitik and E. H. Brandt, Phys. Rev. B **71**, 012510 (2005).
[12] E. H. Brandt and G. P. Mikitik, Phys. Rev. B **76**, 064526 (2007).
[13] G. Blatter, M. V. Feigel'man, V. B. Geshkenbein, A. I. Larkin, and V. M. Vinokur, Rev. Mod. Phys. **66**, 1125 (1994).
[14] E. H. Brandt, Rep. Prog. Phys. **58**, 1465 (1995).
[15] Y. Yeshurun, A. P. Malozemoff, and A. Shaulov, Rev. Mod. Phys. **68**, 911 (1996).
[16] C. P. Bean, Phys. Rev. Lett. **8**, 250 (1962).
[17] E. H. Brandt, Phys. Rev. B **68**, 054506 (2003).
[18] E. H. Brandt, Phys. Rev. B **52**, 15442 (1995).
[19] A. M. Campbell and J. E. Evetts, Adv. Phys. **21**, 199 (1972).
[20] H. Wiesinger, F. Sauerzopf, and H. Weber, Physica C **203**, 121 (1992).
[21] M. Zehetmayer, M. Eisterer, J. Jun, S. M. Kazakov, J. Karpinski, A. Wisniewski, and H. W. Weber, Phys. Rev. B **66**, 052505 (2002).
[22] M. Angadi, A. Caplin, J. Laverty, and Z. Shen, Physica C **177**, 479 (1991).